Journal of Power Sources 196 (2011) 1455–1460

Contents lists available at ScienceDirect

Journal of Power Sources

journal homepage: www.elsevier.com/locate/jpowsour

Vertically aligned carbon nanotube electrodes for lithium-ion batteries

Daniel T. Welna[a,c], Liangti Qu[b], Barney E. Taylor[a,c], Liming Dai[d,**], Michael F. Durstock[a,*]

[a] Materials and Manufacturing Directorate, Air Force Research Laboratory, AFRL/RX, Wright-Patterson AFB, OH 45433, USA
[b] Department of Chemistry, Beijing Institute of Technology, 100081 Beijing, China
[c] UTC, Inc., Beavercreek, OH 45431, USA
[d] Department of Chemical Engineering, Case Western Reserve University, 10900 Euclid Ave., Cleveland, OH 44146 USA

ARTICLE INFO

Article history:
Received 17 June 2010
Received in revised form 2 August 2010
Accepted 3 August 2010
Available online 8 August 2010

Keywords:
Carbon nanotube
Nanostructured electrode
Lithium-ion
Energy storage
Battery

ABSTRACT

As portable electronics become more advanced and alternative energy demands become more prevalent, the development of advanced energy storage technologies is becoming ever more critical in today's society. In order to develop higher power and energy density batteries, innovative electrode materials that provide increased storage capacity, greater rate capabilities, and good cyclability must be developed. Nanostructured materials are gaining increased attention because of their potential to mitigate current electrode limitations. Here we report on the use of vertically aligned multi-walled carbon nanotubes (VA-MWNTs) as the active electrode material in lithium-ion batteries. At low specific currents, these VA-MWNTs have shown high reversible specific capacities (up to 782 mAh g^{-1} at 57 mA g^{-1}). This value is twice that of the theoretical maximum for graphite and ten times more than their non-aligned equivalent. Interestingly, at very high discharge rates, the VA-MWNT electrodes retain a moderate specific capacity due to their aligned nature (166 mAh g^{-1} at 26 A g^{-1}). These results suggest that VA-MWNTs are good candidates for lithium-ion battery electrodes which require high rate capability and capacity.

Published by Elsevier B.V.

1. Introduction

Batteries are one of the most heavily utilized mobile energy sources in today's world. They are used in a wide variety of portable electronics such as cell phones and laptops, hybrid automobiles, and orbiting satellites. Although batteries are employed in a broad range of applications, they continue to experience limitations as energy and power requirements escalate with the evolution of technology. This has led to increased interest in the development of electrode materials and processing capabilities necessary to enable high-performance, next-generation battery systems that can deliver large amounts of energy at high rates [1–4]. Nanostructured materials offer a potential solution to this problem. Due to their nanoscale dimensions and greatly increased surface area compared to conventional electrodes [3–6], increased energy storage capacities and rate capabilities are possible through much faster interfacial and solid-state diffusion kinetics.

A wide variety of nanostructured materials are currently being explored for both the negative and positive battery electrodes [7]. This includes, but is not limited to, cobalt oxide [8] and phospho-olivine [9] nanoparticles, cobalt oxide [10] and silicon [11] nanowires, and iron oxide/copper [12] and tin/copper [13] nanorods. Carbon nanotubes (CNTs) have also been examined as negative electrodes [14–17]. Although CNTs and other negative electrode nanomaterials have been shown to exhibit similar or greater capacities compared to the commercial lithium-ion battery standard of graphite (maximum theoretical capacity of 372 mAh g^{-1}), they do not improve on graphite's moderate rate capability [18]. Studies suggest that aligned CNTs could allow for better contact with the current collector and increased ion diffusivity to significantly improve bulk electron transport properties thereby allowing for improved rate capabilities [19–22]. Recent works by Chen et al. [23], Pushparaj et al. [24], and Masarapu et al. [25] have incorporated aligned CNTs into lithium-ion battery electrodes. However, capacities of 265, 110, and 250 mAh g^{-1}, respectively, were obtained at low discharge rates possibly due to poor electron transport resulting from of poor contact between the CNTs and their current collectors.

In this study, we investigate the electrochemical properties of vertically aligned multi-walled carbon nanotubes (VA-MWNTs) for lithium-ion battery negative electrodes. The VA-MWNTs are supported at their base by a thin nickel metal film, which acts as a support to the nanotubes, helping to maintain their alignment. The nickel film also acts as an excellent current collector due to the intimate contact with the MWNTs. The alignment of the MWNTs in the direction of ion diffusion in a battery cell significantly increases the accessibility of the electrode interior to the electrolyte. The lithium-ion storage capacity and rate capability of the aligned nanotubes are

* Corresponding author. Tel.: +1 937 255 9208; fax: +1 937 255 9157.
** Corresponding author. Tel.: +1 216 368 4151.
E-mail addresses: liming.dai@case.edu (L. Dai), Michael.Durstock@wpafb.af.mil (M.F. Durstock).

0378-7753/$ – see front matter. Published by Elsevier B.V.
doi:10.1016/j.jpowsour.2010.08.003

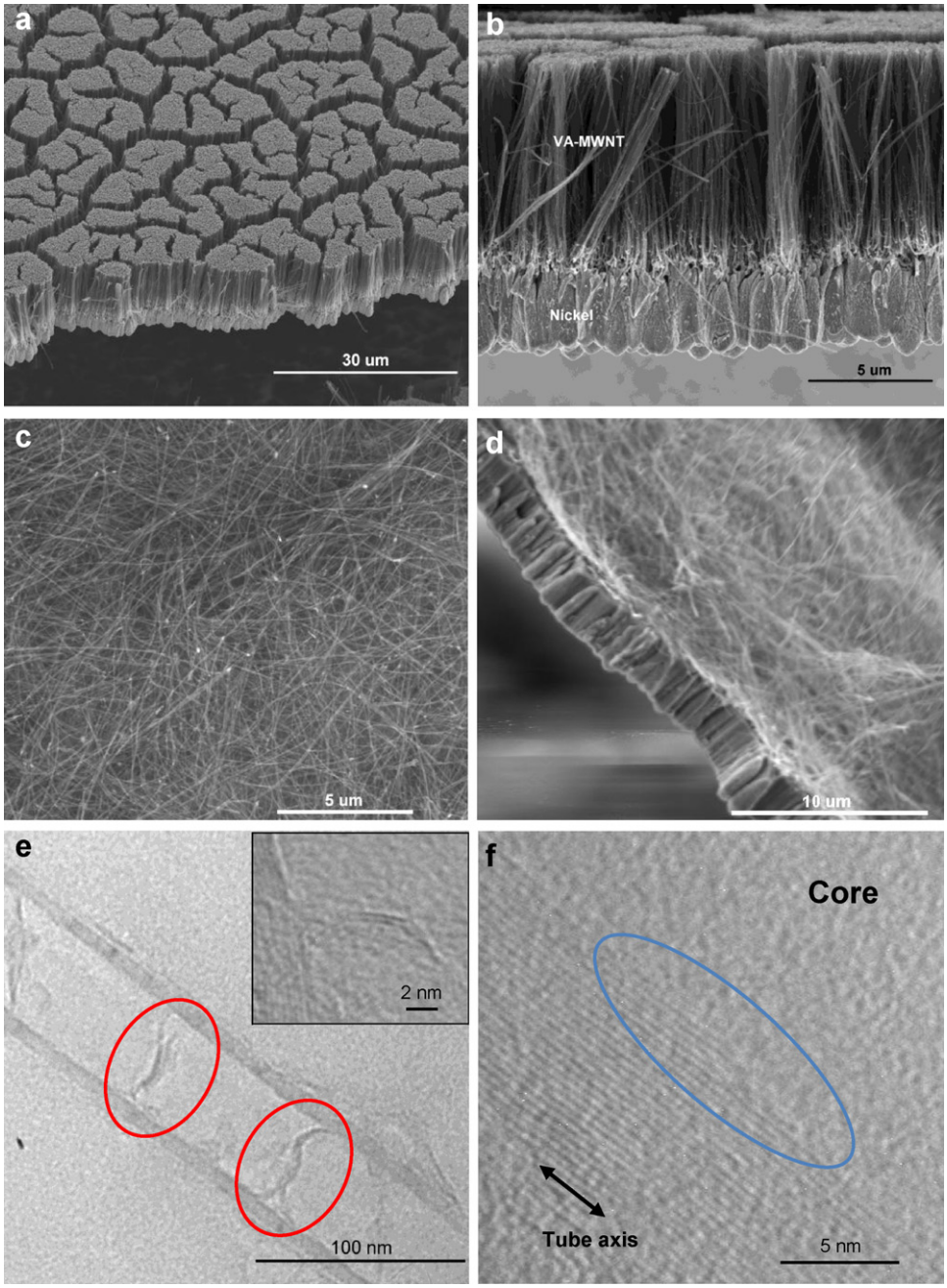

Fig. 1. SEM images of a VA-MWNT (a and b) and a non-aligned MWNT (c and d) electrode. TEM images of a VA-MWNT electrode showing the loose graphene layers (e) and the graphene nanotube edges (f) within the internal nanotube structure.

shown to be significantly improved compared to the non-aligned case.

2. Experimental

Scanning electron microscopy (SEM) and energy dispersive spectroscopy (EDS) were performed on a FEI Quanta environmental scanning electron microscope. X-ray diffraction (XRD) patterns were recorded using Cu Kα radiation on a Bruker AXS D8 Discover spectrometer in transmission mode. Transmission electron microscopy (TEM) was performed on a Philips CM 200 LaB6 transmission electron microscope. Raman spectroscopy was done on a Renishaw inVia Raman microscope. Electrochemical characterization was carried out at room temperature in an argon filled glove box with a two-electrode cell. Lithium metal foil (Aldrich) was used as the counter electrode. The electrodes were separated by a Celgard® 2400 battery membrane soaked in a liquid electrolyte solution consisting of 1.0 M lithium tetrafluoroborate ($LiBF_4$) in ethylene carbonate (EC)/diethyl carbonate (DEC) (1:1, v/v ratio) (Aldrich) solution. The VA-MWNT and non-aligned MWNT electrochemical measurements were performed galvanostatically with voltage limits of 0.02/3.6 V and 0.02/3.0 V *vs.* Li/Li^+, respectively, at various discharge specific currents using a Keithley 2410 Source meter or a Maccor 4300 Battery testing system. All electrochemical measurements were carried out inside an argon gas filled glove box (H_2O and O_2 limit <1 ppm) with a Swagelok® test cell. A standard charge specific current of ~50 mA g^{-1} was utilized to ensure complete lithium-ion extraction unless a lower specific discharge current was employed, in which case the lower value was used for charging. The masses of the VA-MWNT and non-aligned MWNT

electrodes were obtained by subtracting the mass of the nickel film, which was calculated from SEM micrograph dimensions, from the total mass of the CNT and nickel film.

3. Results and discussion

The VA-MWNTs were synthesized via the pyrolysis of iron(II) phthalocyanine (FePc) on a quartz substrate under $Ar_{(g)}/H_{2(g)}$ at 800–1100° C according to published procedures [26,27]. A thin layer (3.5 ± 0.3 μm) of nickel, a non-lithium alloying metal, was sputtered onto the top surface of the VA-MWNTs, followed by treatment with a hydrofluoric acid (HF) solution (10–40%, w/w), producing a free standing film of open tipped VA-MWNTs on nickel. Fig. 1a and b shows SEM images of the nanotube electrodes. Fig. 1e and f shows TEM images of the internal structure of the nanotubes. They were 8.6 ± 0.3 μm in length with an average outer tube diameter of 77 ± 23 nm and wall thicknesses of 10–15 nm. The bunching of the VA-MWNTs, evident in Fig. 1a, results from drying the tubes following the HF treatment step in the transfer of the VA-MWNT film from quartz to a nickel substrate. XRD analysis revealed a well-graphitized material with a graphene interlayer *d*-spacing of 3.35 Å. Additionally, Raman spectroscopy showed prominent features at 1354 cm^{-1}, indicative of the disorder (D) peak usually assigned to the K-point phonons of A_{1g} symmetry typical in polycrystalline graphite, and at 1584 cm^{-1} (G peak), which is common in single graphite crystals and is attributed to the zone centered phonons of $E_{2g}{}^2$ symmetry. The non-aligned MWNTs, shown in Fig. 1c and d, were obtained using the same synthetic procedure as for the VA-MWNTs except that following nanotube growth, the film was treated with HF to remove the quartz substrate. The nanotubes were then dispersed in ethanol by ultrasonication and filtered onto a 1.2 μm PTFE filter. Nickel was then sputtered onto one side of the non-aligned nanotube mat. The non-aligned MWNTs are comparable in tube length, diameter, and wall thickness to the VA-MWNTs.

Electrochemical half-cells were first assembled using lithium metal and VA-MWNTs (without any polymeric binders or conductive carbon additives) as the electrodes. A porous polypropylene film infiltrated with a solution of DEC, EC, and $LiBF_4$ was placed between the electrodes to act as both separator and electrolyte. Galvanostatic cycling measurements were then performed on these cells at a range of different charge/discharge rates. The voltage profile of the VA-MWNT electrodes, shown in Fig. 2a, exhibited a stepwise behavior similar to graphite and other carbonaceous materials during the initial segment of the first discharge [28]. The presence of two declining voltage plateaus, at 1.41 V and 0.77 V, account for the irreversible specific capacity loss (Q_{irr}) and are attributed entirely to the electrolytic degradation of DEC and EC, respectively, which result in the formation of a solid electrolyte interphase (SEI) layer. The formation of this SEI layer is an irreversible process and is critical in creating a stable electrolyte-electrode interface [29]. Similar plateaus are also observed in the non-aligned MWNT electrode as shown in Fig. 3a. These plateaus are clearly recognizable as large peaks in the differential capacity plots of Figs. 2b and 3b ($-dQ/dV$ = discharge, $+dQ/dV$ = charge). It should be noted that these peaks disappear after the first discharge cycle and do not occur in subsequent cycles indicating the complete and stable formation of the SEI layer. The Q_{irr} is fairly high due to the significantly increased surface area of the nanotube films as compared to standard graphite electrodes [4]. SEM images of pristine and cycled VA-MWNT electrodes, as shown in Fig. 4, reveal a conformal SEI coating of the nanotubes as well as SEI particles of various sizes attached to the exposed end and sides of the nanotubes. Energy dispersive spectroscopy (EDS) was utilized to analyze the SEI on the cycled VA-MWNTs which showed the presence of oxygen and fluorine not originally present in the pristine

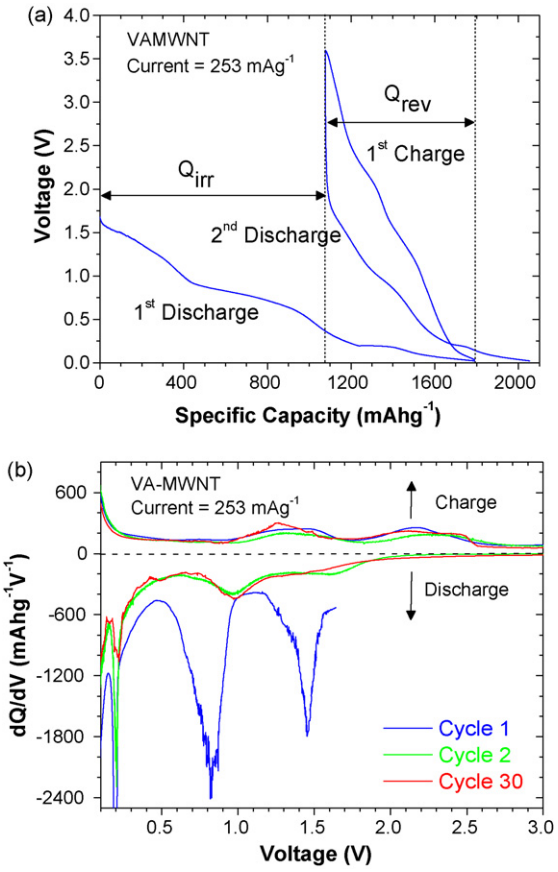

Fig. 2. VA-MWNT voltage profile for the 1st discharge/charge and 2nd discharge cycles (a) and differential capacity plot of the 1st, 2nd and 30th discharge/charge cycles (b).

(pre-cycled) and control VA-MWNT electrode. The control sample, which underwent no cycling, was prepared by evaporating the electrolyte solution from the surface of a pristine VA-MWNT electrode. The presence of oxygen and fluorine in the cycled VA-MWNT electrode clearly indicated the formation of the SEI.

Following the SEI formation during the first discharge cycle, Figs. 2a and 3a show a steady decline until a major plateau at 0.20 V, after which the voltage continues to drop until the discharge voltage limit was reached. The presence of this plateau suggests that a phase transition is occurring which, to the best of our knowledge, is not typically observed in MWNT electrode systems [3,30–33]. Additionally, this behavior seems to disappear in the non-aligned MWNT electrode following the first discharge cycle. This is presumably related to the non-aligned nature of the nanotubes inhibiting the ability of lithium ions to be inserted and extracted from the nanotube electrode. An additional effect of the nanotube alignment, as seen in Figs. 2 and 3, is the electrochemical behavior that occurs at >0.75 V and that is not apparent in the non-aligned MWNTs. From the second through the thirtieth discharge cycles of the VA-MWNT electrode, a peak at 0.96 V was observed along with the peak at 0.20 V (the peak at 0.96 V was presumably present during the first discharge cycle but was masked by the SEI formation). However for the non-aligned MWNT electrode, only the peak at 0.20 V was observed. These peaks are also consistently observed in the charge cycles, indicating that they are not associated with SEI formation, but they occur at higher voltages and with rather significant voltage hysteresis. The 0.96 V discharge peak corresponds to 2.16 V upon charging and the 0.2 V peak corresponds to 1.40 V. There is very little change in these voltages from the second to the thirtieth cycle indicating that a stable and reversible electrochemical process is

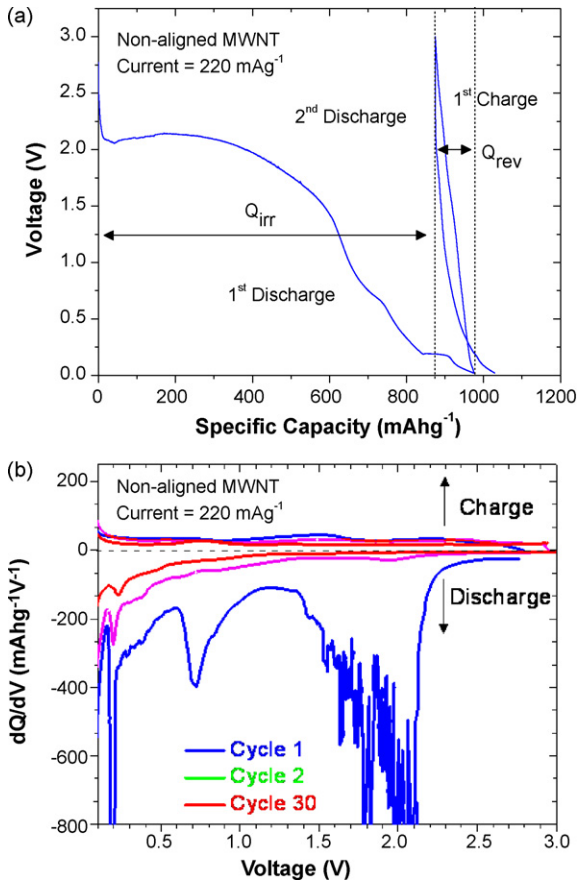

Fig. 3. Non-aligned MWNT voltage profile for the 1st discharge/charge and 2nd discharge cycles (a) and differential capacity plot of the 1st, 2nd and 30th discharge/charge cycles (b).

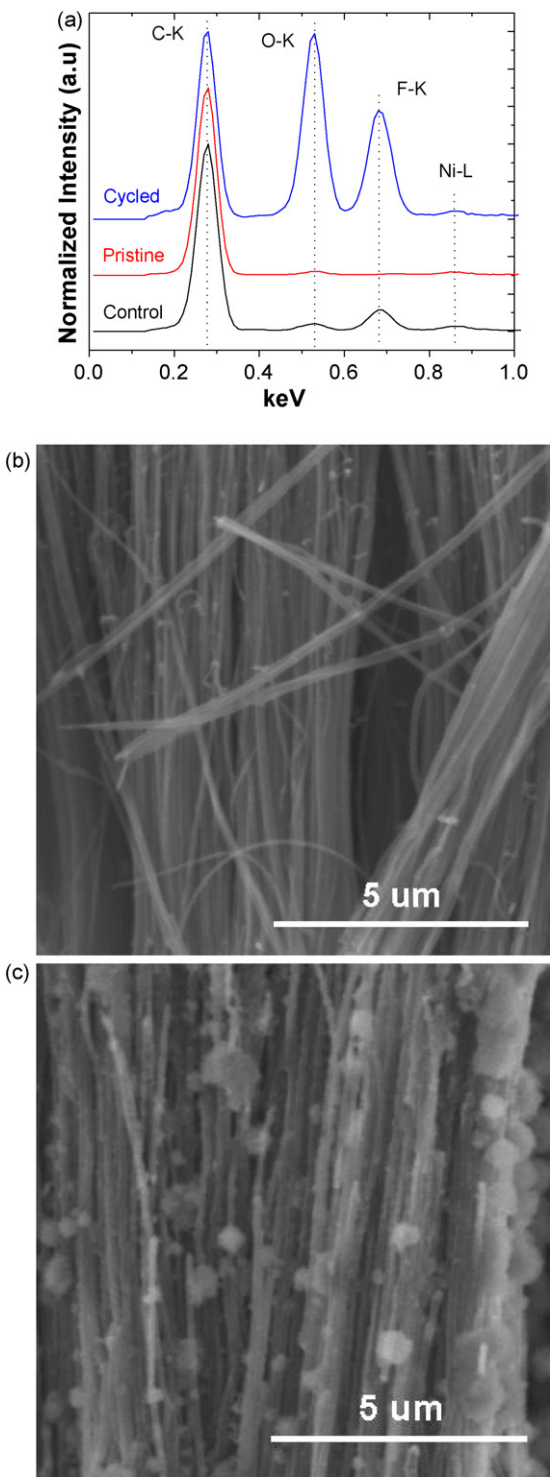

Fig. 4. EDS spectra taken from a pristine, cycled, and control VA-MWNT electrode showing the presence of an SEI layer (a). SEM images of a pristine (b) and a cycled (c) VA-MWNT electrode illustrating a conformal SEI coating and particles on the nanotubes.

taking place. Although the exact nature of the electrochemical process is yet uncertain we believe that it may result from the insertion and extraction of lithium ions into the VA-MWNT cores and into the spaces between the nanotube bundles. A previous study by Yang et al. indicated that lithium ions inserted into the core of CNTs exhibit higher voltage electrochemical behavior around 0.90 V [34]. This behavior is supported by the fact that the non-aligned MWNTs do not exhibit a higher voltage peak in Fig. 3b. The non-aligned nanotubes are not as conducive to ion insertion into the core as are the vertically aligned nanotubes and so no peak is observed.

The cyclability of the vertically aligned nanotubes is significantly enhanced compared to the non-aligned nanotubes as seen in Fig. 5. The specific capacities of both the VA-MWNTs and the non-aligned MWNTs as a function of cycle number are shown in Fig. 5a, while the voltage profiles for these cycles are shown in Fig. 5b and c. After the irreversible capacity loss of the first cycle (Q_{irr}), the reversible capacity (Q_{rev}) of the VA-MWNTs decreases from 980 mAh g^{-1} to a minimum near the tenth cycle, after which it increases slightly and stabilizes near 750 mAh g^{-1}. Q_{rev} for the non-aligned MWNTs, on the other hand, continuously decreases from 158 mAh g^{-1} to 58 mAh g^{-1} by cycle number 34. The alignment of the nanotubes in the direction of ion diffusion allows lithium ions to more readily access the open nanotube ends and significantly increases the Q_{rev} of the VA-MWNTs compared to the non-aligned MWNTs. The TEM images in Fig. 1e and f shows that the internal core of the nanotubes contains irregular structural features such as loose graphene layers (red circles) and graphene nanotube edges (blue circle). These structural features significantly increase the effective surface area of the nanotubes and provide more defect sites at which lithium ions may be adsorbed to the surfaces of loosely bound graphene layers or to hydrogen-containing edge carbon sites [35–37]. The increased storage capacity may also be a result of the intimate contact between each of the individual VA-MWNTs and the nickel metal current collector. The intimate contact ensures that each MWNT maintains electrical continuity to the current collector and is able to participate in the cycling of the electrode. In the case of the non-aligned MWNTs, each nanotube is likely not in contact with the current collector but relies on contact between the nanotubes

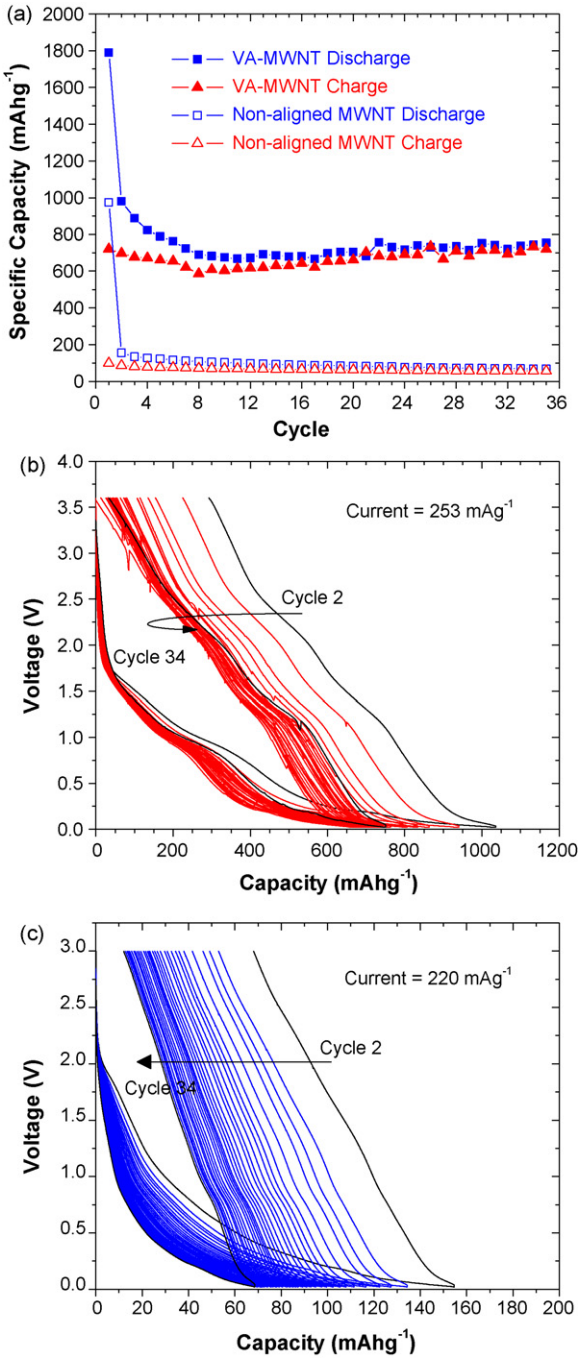

Fig. 5. Specific capacity as a function of cycle for VA-MWNT and non-aligned MWNT electrodes at similar discharge rates (a). Voltage profile of cycles 2–34 for VA-MWNT (b) and non-aligned MWNT (c) electrodes.

resulting in a higher effective resistance and lower overall storage capacity.

The rate capability of the aligned and non-aligned nanotubes is shown in Fig. 6. The largest value of Q_{rev} for the VA-MWNTs was 782 mAh g^{-1} at 57 mA g^{-1}, which is more than twice the maximum theoretical specific capacity of graphite. The capacity decreased as the current was increased presumably due to the kinetic limitations of ion diffusion that come into play at high current densities [38]. Nevertheless, high reversible specific capacities were maintained even at very high discharge rates. Q_{rev} did not fall below 166 mAh g^{-1} until discharge rates exceeded 26 A g^{-1}. It should be noted that we believe the very high discharge rates are due to the

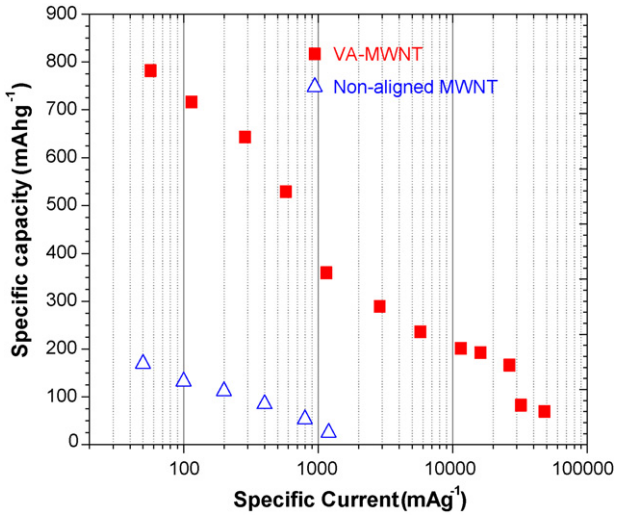

Fig. 6. Specific capacity as a function of specific current for VA-MWNT and non-aligned MWNT electrodes.

small dimensions and weight of the nanotube electrodes. When comparing the VA-MWNTs' volumetric capacity, 395 mAh cm^{-3} (corresponds to 782 mAh g^{-1}), to the theoretical maximum volumetric capacity of graphite (833 mAh cm^{-3}), much higher material densities would be required to realize practical electrodes with high total capacities. Various approaches to increase the VA-MWNTs material density are currently being explored. The non-aligned MWNT electrodes exhibited rate capabilities that were considerably lower than the VA-MWNT electrodes. The highest value of Q_{rev} was 169 mAh g^{-1} at 50 mA g^{-1} and this declined to 26 mAh g^{-1} at 1200 mA g^{-1}. The higher rate capability of the VA-MWNT electrodes is a direct result of the nanotube alignment and supports the notion of lithium ions accessing the interior of the nanotube.

4. Conclusions

We have shown that vertically aligned MWNT electrodes can lead to higher storage capacities and significantly higher rate capabilities compared to graphite. The rate capability reported here is substantially greater than any value previously reported for carbon nanotube electrodes [14–17,23,24,30–33,35,37] and emphasizes the role that structural order can play in electrode performance. Alignment of the MWNTs in the direction of ion diffusion led to an increase in both the storage capacity and the rate capability. These results support the notion that lithium ions access the internal core of the nanotubes which contain loosely bound graphene layers and graphene nanotube edges. These structural features increased the effective surface area of the electrode and presumably provide defect sites with which the lithium ions interact. Additionally, the intimate contact between each of the vertically aligned nanotubes and the nickel metal current collector provides a low resistance pathway allowing for effective connectivity throughout the electrode. Furthermore, if the material density can be increased and the irreversibly specific capacity decreased, the large reversible specific capacity of the aligned carbon nanotubes and their ability to maintain moderate specific capacities at very high discharge rates make this concept attractive for high power lithium-ion batteries.

Acknowledgements

We acknowledge the funding for this research by the Air Force Office of Scientific Research under contract numbers FA8650-D-5807 and FA9550-09-1-0331, and we thank Dr. Lawrence

Drummy for his assistance with carrying out transmission electron microscopy.

References

[1] J.-M. Tarascon, M. Armand, Nature 414 (2001) 359.
[2] D.R. Sadoway, A.M. Mayers (Eds.), MRS Bull. 27 (2002) 590.
[3] M. Armand, J.-M. Tarascon, Nature 451 (2008) 652.
[4] P.G. Bruce, B. Scrosati, J.-M. Tarascon, Angew. Chem. Int. Ed. 47 (2008) 2930.
[5] A.S. Arico, P. Bruce, B. Scrosati, J.-M. Tarascon, W. van Schalkwijk, Nat. Mater. 4 (2005) 366.
[6] Y.-G. Guo, J.-S. Hu, L.-J. Wan, Adv. Mater. 20 (2008) 2878.
[7] M. Kim, J. Cho, Adv. Funct. Mater. 19 (2009) 1497.
[8] P. Poizot, S. Laruelle, S. Grugeon, L. Dupont, J.-M. Tarascon, Nature 407 (2000) 496.
[9] P. Gibot, M. Casas-Cabanas, L. Laffont, S. Levasseur, P. Carlach, S. Hamelet, J.-M. Tarascon, C. Masquelier, Nat. Mater. 7 (2008) 741.
[10] K.T. Nam, D.-W. Kim, P.J. Yoo, C.-Y. Chiang, N. Meethong, P.T. Hammond, Y.-M. Chiang, A.M. Belcher, Science 312 (2006) 885.
[11] C.K. Chan, H. Peng, G. Liu, K. McIlwrath, X.F. Zhang, R.A. Huggins, Y. Cui, Nat. Nanotechnol. 3 (2008) 31.
[12] P.L. Taberna, S. Mitra, P. Poizot, P. Simon, J.-M. Tarascon, Nat. Mater. 5 (2006) 567.
[13] L. Bazin, S. Mitra, P.L. Taberna, P. Poizot, M. Gressier, M.J. Menu, A. Barnabé, P. Simon, J.-M. Tarascon, J. Power Sources 188 (2009) 578.
[14] G.X. Wang, J. Ahn, J. Yao, M. Lindsey, H.K. Liu, S.X. Dou, J. Power Sources 119–121 (2003) 16.
[15] X.X. Wang, J.N. Wang, H. Chany, Y.F. Zhang, Adv. Funct. Mater. 17 (2007) 3613.
[16] Q. Wang, L. Chen, X. Huang, Electrochem. Solid-State Lett. 37 (2002) A188.
[17] E. Frackowiak, S. Gautier, H. Gaucher, S. Bonnamy, F. Beguin, Carbon 37 (1999) 61.
[18] H. Buqu, D. Goers, M. Holzapfel, M.E. Spahr, P. Novák, J. Electrochem. Soc. 152 (2005) A474.
[19] D.N. Futaba, K. Hata, T. Yamada, T. Hiraoka, Y. Hayamizu, Y. Kakudate, O. Tanaike, H. Hatori, M. Yumura, S. Iijima, Nat. Mater. 5 (2006) 987.
[20] J. Zhao, Q.Y. Gao, Y. Yang, Chem. Phys. Lett. 358 (2002) 77.
[21] Y. Honda, T. Haramoto, M. Takeshige, H. Shiozaki, T. Kitamura, M. Ishikawa, Electrochem. Solid-State Lett. 10 (2007) A106.
[22] H. Zhang, G. Cao, Y. Yang, Z. Gu, J. Electrochem. Soc. 155 (2008) K19.
[23] J. Chen, Y. Liu, A.I. Minett, C. Lynam, J. Wang, G.G. Wallace, Chem. Mater. 19 (2007) 3595.
[24] V.L. Pushparaj, M.M. Shaijumon, A. Kumar, S. Murugesan, L. Ci, R. Vajtai, R.J. Linhardt, O. Nalamasu, P.M. Ajayan, PNAS 104 (2007) 13574.
[25] C. Masarapu, V. Subramaniam, H. Zhu, B. Wei, Adv. Funct. Mater. 19 (2009) 1008.
[26] S. Huang, L. Dai, A.W.H. Mau, J. Phys. Chem. B 103 (1999) 4223.
[27] D.-C. Li, L. Dai, S. Huang, A.W.H. Mau, Z.L. Wang, Chem. Phys. Lett. 316 (2000) 349.
[28] S. Flandrois, B. Simon, Carbon 37 (1999) 165.
[29] P.B. Balbueng, Y. Wang (Eds.), Lithium-Ion Batteries: Solid Electrolyte Interphase, Imperial College Press, London, 2004.
[30] G. Maurin, Ch. Bousquet, F. Henn, P. Bernier, R. Almairac, B. Simon, Chem. Phys. Lett. 312 (1999) 14.
[31] G. Wu, C. Wang, X. Zhang, H. Yang, Z. Qi, P. He, W. Li, J. Electrochem. Soc. 146 (1999) 1696.
[32] S. Yang, J. Huo, H. Song, X. Chen, Electrochim. Acta 53 (2008) 2238.
[33] Z. Yang, Y. Feng, Z. Li, S. Sang, Y. Zhou, L. Zeng, J. Electron. Chem. 580 (2005) 340.
[34] Z. Yang, H. Wu, Solid State Ionics 143 (2001) 173.
[35] J.R. Dahn, T. Zheng, Y. Liu, J.S. Xue, Science 270 (1995) 590.
[36] B. Gao, A. Kleinhammes, X. Tang, C. Bower, L. Fleming, Y. Wu, O. Zhou, Chem. Phys. Lett. 307 (1999) 153.
[37] Z. Yang, H. Wu, Mater. Chem. Phys. 71 (2001) 7.
[38] D. Linden, T.B. Reddy, Handbook of Batteries, 3rd ed., McGraw-Hill Co., Inc., New York, 2005.